Density Functional Theory and ab Initio Direct Dynamics Studies on the Hydrogen Abstraction Reactions of Chlorine Atoms with $CHCl_{3-n}F_n$ (n = 0, 1, and 2) and CH_2Cl_2

Jing-Fa Xiao, Ze-Sheng Li,* Yi-Hong Ding, Jing-Yao Liu, Xu-Ri Huang, and Chia-Chung Sun

Institute of Theoretical Chemistry, State Key Laboratory of Theoretical and Computational Chemistry, Jilin University, Changchun 130023, P. R. China

Received: September 5, 2001; In Final Form: October 30, 2001

The dynamical properties of the hydrogen abstraction reactions from halomethanes of $CHCl_{3-n}F_n$ (n = 0−2) and CH_2Cl_2 with Cl atoms in the temperature range 200−700 K are investigated theoretically. The minimum energy paths (MEPs) of these reactions are calculated at the BH&H-LYP/6-311G(d,p) level, and the energies along the MEPs are further refined at the QCISD(T)/6-311+G(d,p) (single-point) level. For the title reactions, the theoretical rate constants by using improved canonical variational transition state theory incorporating small-curvature tunneling correction are in good agreement with available experimental results. It is shown that the vibrational adiabatic potential energy curves for these reactions have two barriers, a situation similar to the analogous $CH_3X + Cl$ (X = F, Cl, Br) reaction. For these reactions, the small-curvature tunneling effects are found to be small and the variational effects except for the $CHCl_3 + Cl$ reaction are found to be small over the temperature range considered.

Introduction

The H-abstraction reactions from halogen-substituted hydrocarbons by chlorine atom attack in the gas phase have been the subject of many experimental studies. The importance of halocarbons in atmospheric chemistry is well established.[1,2] Chloromethanes are known to be important atmospheric species and should be responsible for the depletion of the ozone layer in the stratosphere and for the greenhouse effects. These reactions play an important role in the processes of industrial chlorination and in the incineration of hazardous halogenated wastes.[3] In this paper, we focus our attention on the rate constants of four halogen-substituted hydrogen-abstraction reactions $CHCl_3 + Cl \rightarrow CCl_3 + HCl$, $CHCl_2F + Cl \rightarrow CCl_2F + HCl$, $CHClF_2 + Cl \rightarrow CClF_2 + HCl$, and $CH_2Cl_2 + Cl \rightarrow CHCl_2 + HCl$. There have been some experimental studies available in the literature concerning rate constants for the reactions of $CHCl_3$,[4−11] CH_2Cl_2,[4−8,11−13] $CHCl_2F$,[9,14,15] and $CHClF_2$.[9,14−16] For the reactions of $CHCl_2F$ and $CHClF_2$, only one experimental result[9] shows the temperature dependence of rate constants. For the reactions $CHCl_3$ and CH_2Cl_2, the agreement for most of the experimental data is excellent.

In contrast to the large number of experimental data, theoretical studies on the kinetic parameters of these reactions are rather limited. In 1988, Tschuikow-Roux et al.[12] reported the semiempirical bond energy−bond order (BEBO) study on the $CH_2Cl_2 + Cl \rightarrow CHCl_2 + HCl$ reaction and gave the kinetic parameters by using conventional transition state theory (TST). In 1994, Rayez et al.[17] obtained the 298 K rate constants for the title four reactions at the HF/6-31G(d,p) level followed by the BAC-MP4 single-point energy calculations and one-dimensional (1D) tunneling correction. Generally, their calculated rate constants are in quantitative agreement with the experimental data. Yet, their predicted reactivity trend $k(CHCl_3 + Cl) > k(CH_2Cl_2 + Cl)$ qualitatively contradicts with the experimental results. We note that Rayez et al. did not calculate the analytical potential energy surface and just made a crude estimate of a 1D approach of the tunneling factor in these reactions. In addition, they only reported the rate constants at room temperature. The aim of this paper is to perform a direct ab initio dynamics study at a relatively higher level on the rate constants of the four hydrogen abstraction reactions by Cl atoms over the temperature range 200−700 K in order to obtain more precise results.

Calculation Methods

It has been previously shown[18−21] that the combination of Becke's half-and-half (BH&H)[22] with Lee−Yang−Parr (LYP)[23] nonlocal correlation functionals can be used cost-effectively to calculate the geometries and frequencies particularly for open-shell systems. In the present work, the equilibrium geometries and frequencies of the stationary points (reactants, products, and transition states) are calculated by using the BH&H-LYP method with the 6-311G(d,p) basis set by using Gaussian 98 program package.[24] At the same level, the minimum energy path (MEP) is obtained by intrinsic reaction coordinate theory (IRC) with a gradient step size of 0.05 $(amu)^{1/2}$ bohr. Furthermore, selected points along the MEP, the force constant matrices as well as the harmonic vibrational frequencies are obtained. To obtain more accurate information on energy, the quadratic configuration interaction with single and double substitutions with a triple contribution [QCISD(T)][25] calculations are performed using the 6-311+G(d,p) basis set at the BH&H-LYP MEP geometries.

By means of the POLYRATE-Version 8.4.1 program,[26] the theoretical rate constants are calculated using the conventional transition state theory (TST) and the improved canonical variational transition state theory (ICVT) incorporating small-curvature tunneling correction (SCT) method proposed by Truhlar and co-workers.[27,28] Improved canonical variational transition state theory rate constants, $k^{ICVT}(T)$, at fixed temperature (T) by minimizing improved generalized transition state

10.1021/jp013405u CCC: $22.00
Published on Web 12/07/2001

theory rate constant, $k^{IGT}(T,s)$, with respect to the dividing surface at s is expressed as

$$k^{ICVT}(T) = \min_s k^{IGT}(T,s)$$

The improved generalized transition state theory rate constant k^{IGT} for temperature T and dividing surface at s is

$$k^{IGT}(T,s) = \frac{\sigma Q^{IGT}(T,s)}{\beta h Q^{R}(T)} \exp(-\beta V_{MEP}(s))$$

In this equation, s is the location of the improved generalized transition state on the IRC; σ is the symmetry factor accounting for the possibility of two or more symmetry-related reaction paths; β equals $(k_B T)^{-1}$ where k_B is Boltzmann's constant, h is Plank's constant; $Q^R(T)$ is the reactant's partition function per unit volume, excluding symmetry numbers for rotation; $V_{MEP}(s)$ is the classical energy along the MEP overall zero of energy at the reactant. $Q^{IGT}(T,s)$ is the partition function of the improved generalized transition state at s along the MEP. To include tunneling effect, the ICVT rate constant is multiplied by the small-curvature tunneling (SCT) approximation, which is denoted as $k^{ICVT/SCT}(T)$. The rate constants are then calculated at 200−700 K temperatures using the mass-scaled Cartesian coordinate. The Euler single-step integrator with a step size of 0.0001 $(amu)^{1/2}$ bohr is used to follow the MEP, and the generalized normal-mode analysis is performed in every 0.01 $(amu)^{1/2}$ bohr.

Results and Discussions

A. Stationary Points. The optimized geometric parameters of the reactants ($CHCl_3$, $CHCl_2F$, $CHClF_2$, and CH_2Cl_2), and products (CCl_3, CCl_2F, $CClF_2$, $CHCl_2$, and HCl) at the BH&H-LYP/6-311G(d,p) level of theory are shown in Table 1. The available experimental values[29,30] are also listed for comparison. From Table 1 we can see that the largest deviation of the theoretical bond lengths differing from the experimental values is 0.035 Å (r(C−F) for $CHCl_2F$) and the largest deviation of the bond angles is 2.8° for ∠ClCCl of CCl_3. It is obvious that the theoretical geometric parameters are in good agreement with the experimental data.[29,30]

Geometric parameters of the transition state structures for the four hydrogen abstraction reactions are listed in Table 2. To reflect the reactant- or product-like character of the forming transition state, we employ the parameter L,[17] which is the ratio between the elongation of the C−H′ bond and the elongation of the Cl−H′ bond, $L = \delta r(C-H')/\delta r(Cl-H')$. For the $CHCl_3$ + Cl reaction, the transition state has C_{3v} symmetry and $L < 1$. For the remaining three reactions, the transition states have C_s symmetry, and the angles between the breaking C−H′ bond and the nascent H′-Cl bond (∠Cl′H′C) for three reactions are about 175° with $L > 1$.

Table 3 gives the harmonic vibrational frequencies of the reactants, products, and transition states at the BH&H-LYP/6-311G(d,p) level as well as the corresponding experimental results.[31,32] For the species of reactants and products, the calculated frequencies are in good agreement with the experimental values with the largest deviation of 8%. For each reaction, the transition state has only one imaginary frequency.

The reaction enthalpies and classical barrier heights calculated at the QCISD(T)//BH&H-LYP level with ZPE correction are listed in Table 4. For the $CHCl_3$ + Cl, $CHCl_2F$ + Cl, $CHClF_2$ + Cl, and CH_2Cl_2 + Cl reactions, the calculated reaction enthalpies at temperature 298 K are −6.3, −2.5, +1.5, and −4.3 kcal/mol, respectively, which are in reasonable agreement with the corresponding experimental values of −8.4, −4.9, +0.6, and −5.2 kcal/mol.[33] Thus, the reaction exothermicity decreases in the order $CHCl_3$ > CH_2Cl_2 > $CHCl_2F$ > $CHClF_2$. The classical barrier heights of the $CHCl_3$ + Cl, $CHCl_2F$ + Cl, $CHClF_2$ + Cl, and CH_2Cl_2 + Cl reactions are 0.9, 3.0, 6.2, and 1.8 kcal/mol, respectively. The increase of the classical barrier height for the H-abstraction on the order of $CHCl_3$ < CH_2Cl_2 < $CHCl_2F$ < $CHClF_2$ is just the opposite of the reaction exothermicity changes. The increasing classical barrier heights for the reactions $CHCl_3$ + Cl, CH_2Cl_2 + Cl, $CHCl_2F$ + Cl, and $CHClF_2$ + Cl are also consistent with the increasing dissociation energies of the breaking C−H′ bonds within the reactants $CHCl_3$ + Cl, CH_2Cl_2 + Cl, $CHCl_2F$ + Cl, and $CHClF_2$ + Cl; i.e., the corresponding D(C−H′) values are 94.1, 96.9, 97.9, and 101.6 kcal/mol.[17]

TABLE 1: Calculated and Experimental Geometrical Parameters (Distances in Ångstroms and Angles in Degrees) of Stable Structures

species	geometrical params	BH&H-LYP/6-311G(d,p)	expt
$CHCl_3$ (C_{3v})	r(CH)	1.0738	1.100[a]
	r(CCl)	1.7665	1.758
	∠ClCH	107.5	107.5
CCl_3 (C_s)	r(CCl)	1.7117	1.740[b]
	∠ClCCl	117.2	120.0
	τ(ClClCCl)	147.5	
$CHCl_2F$ (C_s)	r(CH)	1.0763	1.090[a]
	r(CCl)	1.7648	1.750
	r(CF)	1.3315	1.367
	∠ClCH	108.3	109.8
	∠FCH	109.8	
	τ(ClCHF)	119.1	
CCl_2F (C_s)	r(CCl)	1.7198	
	r(CF)	1.3106	
	∠ClCF	109.7	
	τ(ClCFCl)	137.1	
$CHClF_2$ (C_s)	r(CH)	1.0788	1.090[a]
	r(CCl)	1.7674	1.740
	r(CF)	1.3255	1.350
	∠ClCH	109.0	1.07.0
	∠FCH	110.2	
	τ(FCHCl)	120.2	
$CClF_2$ (C_s)	r(CCl)	1.7302	
	r(CF)	1.3061	
	∠FCCl	113.7	
	τ(FCClF)	127.8	
CH_2Cl_2 (C_{2v})	r(CH)	1.0762	1.068[a]
	r(CCl)	1.7715	1.772
	∠HCH	111.7	112.0
	∠HCCl	108.0	
$CHCl_2$ (C_s)	r(CH)	1.0714	
	r(CCl)	1.7049	
	∠HCCl	117.1	
	τ(ClCHCl)	151.2	
HCl	r(HCl)	1.2757	1.275[a]

[a] Eperimental values from ref 29. [b] Experimental values from ref 30.

B. Minimum Energy Path. The changes of bond lengths along the IRC for the Cl reaction with $CHCl_3$ are plotted in Figure 1. It is easily seen that with the proceeding of this reaction, the active C−H′ (breaking) and Cl−H′ (forming) bond lengths change very smoothly up to about $s = -0.45$ $(amu)^{1/2}$ bohr. After that, both bonds change rapidly up to about $s = 0.5$ $(amu)^{1/2}$ bohr, and later, the changes become slow again. However, the lengths of the other bond show nearly no change during the entire reaction processes. For the remaining three reactions, i.e., $CHCl_2F$ + Cl, $CHClF_2$ + Cl, and CH_2Cl_2 + Cl, the bond length changes along the IRC are similar to reaction $CHCl_3$ + Cl.

TABLE 2: Optimized Geometrical Parameters (distances in Ångstroms and Angles in Degrees) of the Transition States for Hydrogen Abstraction Reactions of $CHCl_3$, $CHCl_2F$, $CHClF_2$, and CH_2Cl_2 by Cl Atoms at the BH&H-LYP/6-311G(d,p) Level

geometrical params	Cl···H···CCl_3 (C_{3v})	Cl···H···CCl_2F (C_s)	Cl···H···$CClF_2$ (C_s)	Cl···H···$CHCl_2$ (C_s)
r(CH′)	1.2923	1.3304	1.3807	1.3230
r(CH)				1.0777
r(CCl)	1.7350	1.7297	1.7286	1.7249
r(CF)		1.3120	1.3038	
∠ClCH	104.4	105.6	106.7	106.6
∠FCH		105.3	106.2	
τ(ClCHCl)	120.0			124.2
τ(ClCHF)		118.4	121.1	
r(H′Cl′)	1.5318	1.4949	1.4574	1.5069
∠Cl′H′C	180.0	175.0	175.1	174.9
$L = \delta r$(CH′)/δr(H′Cl)	0.853	1.159	1.614	1.067

TABLE 3: Calculated and Experimental Frequencies (cm^{-1}) at Stationary Points for the Four Reactions

species	BH&H-LYP/6-311G(d,p)	expt
$CHCl_3$	277, 277, 384, 696, 803, 803, 1309, 1309, 3289	261, 261, 363, 680, 774, 774, 1220, 1220, 3034[a]
CCl_3	289, 289, 332, 508, 933, 933	266, 266, -, 487, 898, 898[b]
Cl···H···CCl_3	1443*i*, 92, 92, 237, 287, 287, 448, 761, 863, 863, 1085, 1085	
$CHCl_2F$	291, 387, 476, 764, 837, 1172, 1329, 1408, 3271	270, 368, 455, 741, 806, 1079, 1242, 1313, 3023[a]
CCl_2F	297, 401, 476, 632, 905, 1246	747, 919, 1208[b]
Cl···H···CCl_2F	1424*i*, 89, 107, 247, 306, 402, 527, 834, 909, 1059, 1083, 1233	
$CHClF_2$	382, 429, 624, 837, 1182, 1219, 1395, 1452, 3258	400, 417, 598, 812, 836, 1108, 1312, 1350, 3024[a]
$CClF_2$	381, 440, 620, 799, 1228, 1309	599, 761, 1148, 1208[b]
Cl···H···$CClF_2$	1332*i*, 91, 113, 278, 386, 454, 673, 909, 1015, 1021, 1234, 1320	
CH_2Cl_2	298, 738, 783, 936, 1238, 1362, 1516, 3223, 3302	282, 717, 748, 898, 1158, 1268, 1467, 2999, 3054[a]
$CHCl_2$	317, 485, 779, 921, 1305, 3324	902, 1226[b]
Cl···H···$CHCl_2$	1374*i*, 89, 157, 308, 402, 794, 866, 918, 1037, 1191, 1314, 3259	
HCl	3046	2991[a]

[a] Experimental values from ref 31. [b] Experimental values from ref 32.

TABLE 4: Reaction Enthalpies (ΔH°_{298}) and Forward Classical Barrier Height (ΔE^f) (kcal/mol) with ZPE Correction for the Four Reactions

		BH&H-LYP[a]	QCISD(T)//DFT[b]	expt[c]
$CHCl_3 + Cl \rightarrow CCl_3 + HCl$	ΔH°_{298}	−5.7	−6.3	−8.4
	ΔE^f	4.6	0.9	
$CHCl_2F + Cl \rightarrow CCl_2F + HCl$	ΔH°_{298}	−1.7	−2.5	−4.9
	ΔE^f	5.7	3.0	
$CHClF_2 + Cl \rightarrow CClF_2 + HCl$	ΔH°_{298}	2.1	1.5	0.6
	ΔE^f	7.7	6.2	
$CH_2Cl_2 + Cl \rightarrow CHCl_2 + HCl$	ΔH°_{298}	−3.1	−4.3	−5.2
	ΔE^f	4.3	1.8	

[a] Calculated by using the 6-311G(d,p) basis set. [b] Single point QCISD(T)/6-311+G(d,p) energy calculations at the BH&H-LYP/6-311G(d,p) geometries. [c] The experimental values from ref 33.

Figure 2a−d depict the classical potential energy curves ($V_{MEP}(s)$) and the ground-state vibrational adiabatic potential energy curves ($V_a^G(s)$) as functions of the intrinsic reaction coordinate s at the QCISD(T)//BH&H-LYP level together with the zero-point energy curves (ZPE(s)) for the four reactions. We can interestingly find that for each of these reactions, the ground-state vibrational adiabatic potential surface has two barriers, one higher barrier at the entrance valley and another one at the transition state ($s = 0$ (amu)$^{1/2}$ bohr) of the MEP. According to the expression $V_a^G(s) = V_{MEP}(s) + ZPE(s)$, the nonregular V_a^G shape may be attributed to the combination of two different factors: the low-energy barrier and the relatively large early drop of the zero-point energies (ZPE) prior to the saddle point zone.[34] Specifically, when the large early drop of ZPE is combined with a broad V_{MEP} that has a low classical barrier height, a large variational effect will be caused. Figure 2a−d show that the reaction $CHCl_3 + Cl$ has a flater V_{MEP} than reactions $CHCl_2F + Cl$, $CHClF_2 + Cl$, and $CH_2Cl_2 + Cl$. This suggests that among the four reactions, $CHCl_3 + Cl$ may have the largest variational effect, as will be confirmed by the rate constant calculations in section 3.C. Note that such a two-barrier shape of V_a^G has been revealed for the analogous $CH_3X + Cl$ (X = F,[34] Cl,[35] Br[35]) reactions.

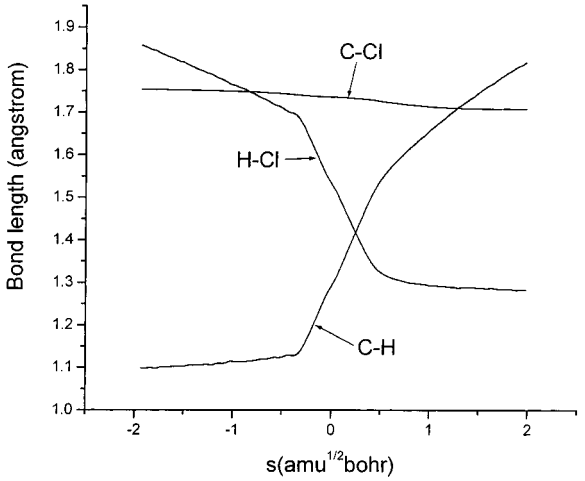

Figure 1. Changes of the bond lengths along the BH&H-LYP/6-311G-(d,p) minimum energy path for the $CHCl_3 + Cl \rightarrow CCl_3 + HCl$ reaction plotted vs the reaction coordinate s in the mass weighted coordinates.

C. Rate Constants. ICVT rate calculations including small-curvature tunneling (SCT) contribution are carried out for the forward direction of the four H-abstraction reactions in the temperature range 200−700 K. Figure 3a−d displays the calculated rate constants and experimental results for the four H-abstraction reactions. For the reaction $CHCl_3 + Cl \rightarrow CCl_3 + HCl$ (see Figure 3a), there are seven experimental measurements[4,5,7−11] on the rate constants, which agree well with each other. The numerical agreement between our ICVT/SCT rate constants and the experimental ones is very good, i.e., the k(ICVT/SCT)/k(expt) falls within the range 0.5−2. Yet, the

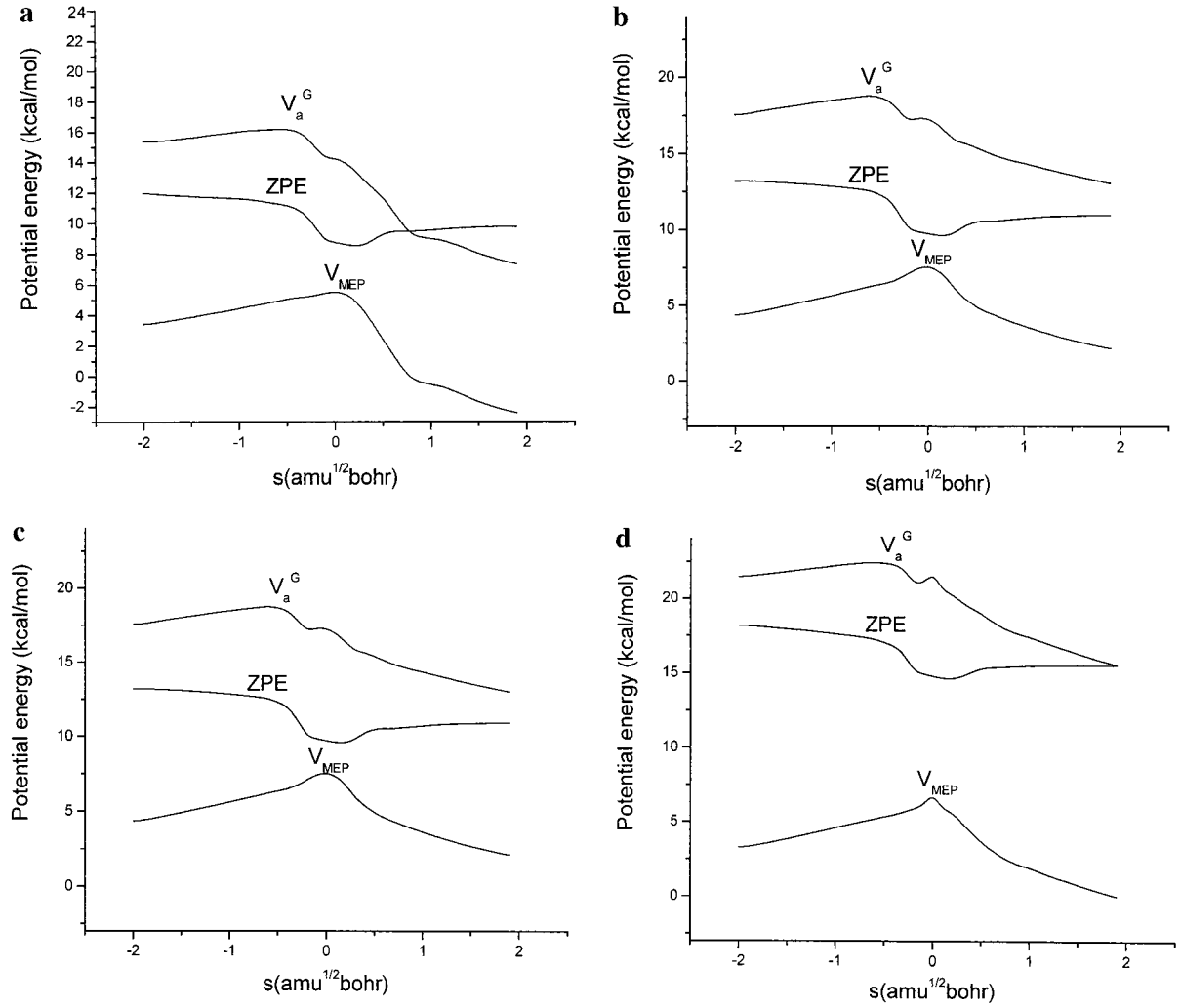

Figure 2. Classical potential energy (V_{MEP}), zero-point energies (ZPE), and vibrational adiabatic potential energy (V_a^G) as a function of the reaction coordinate, *s*, at the QCISD(T)//BH&H-LYP level for the (a) $CHCl_3 + Cl \rightarrow CCl_3 + HCl$, (b) $CHCl_2F + Cl \rightarrow CCl_2F + HCl$, (c) $CHClF_2 + Cl \rightarrow CClF_2 + HCl$, and $CH_2Cl_2 + Cl \rightarrow CHCl_2 + HCl$ reactions.

theoretical temperature dependence of the rate constants is somewhat steeper than that of the measured ones.[4,5,9,11] For the $CHCl_2F + Cl \rightarrow CCl_2F + HCl$ and $CHClF_2 + Cl \rightarrow CClF_2 + HCl$ reactions (see Figure 3b,c), there is only one experimental result[9] that gives the temperature dependence of rate constants and the other experimental results are just measured at 298 K. Our theoretical rate constants are in reasonable agreement with available experimental ones[9] and the ratio k(ICVT/SCT)/k(expt) is within 2−4 for the $CHCl_2F$ reaction and 0.2−0.5 for the $CHClF_2$ reaction in the measured temperature range. The ICVT/SCT slope is in general agreement with the curved experimental plot. Finally, for the $CH_2Cl_2 + Cl \rightarrow CHCl_2 + HCl$ reaction (see Figure 3d), there are seven available experiments[4,5,7,8,11−13] about the rate constants, and these experimental values agree well with each other except for the rate constant obtained by Clyne et al.,[5] which was somewhat larger than that of the other ones. The rate constant by Clyne et al.[5] is 7.52×10^{-13} cm^3 molecule^{-1} s^{-1} and the other ones are about 3.25×10^{-13} cm^3 molecule^{-1} s^{-1} at 298 K, which is in good agreement with our result 3.87×10^{-13} cm^3 molecule^{-1} s^{-1}. From Figure 3d, we can see that our calculated rate constants are in excellent agreement with the experimental values and the ratio k(ICVT/SCT)/k(expt) is in the range 0.7−1.2.

From Table 5 where our ICVT and ICVT/SCT rate constants for the four forward reactions are listed, we can find that both k values decrease in the order of $CH_2Cl_2 > CHCl_3 > CHCl_2F > CHClF_2$. Such a reactivity trend of these reactions is well consistent with the experimental fact, the measured 298 K values of k by Orlando[11] are 3.25×10^{-13} and 1.19×10^{-13} cm^3 molecule^{-1} s^{-1} for CH_2Cl_2 and $CHCl_3$ reactions, respectively, and those by Talhaoui[9] are 7.6×10^{-14}, 1.9×10^{-14}, and 1.4×10^{-15} cm^3 molecule^{-1} s^{-1} for $CHCl_3$, $CHCl_2F$, and $CHClF_2$ reactions, respectively. It should be pointed out that Rayez et al.[17] have calculated the 298 K rate constants for the $CHCl_3$ and CH_2Cl_2 reactions to be 2.4×10^{-13} and 1.3×10^{-13} cm^3 molecule^{-1} s^{-1}, respectively, at the BAC-MP4//HF/6-31G(d,p) level, which yields a reactivity trend $k(CHCl_3) > k(CH_2Cl_2)$. Surely, their obtained reactivity trend is quite different from available experimental results and our calculations. The possible reason may be that Rayez et al. just performed TST calculations followed by a crude estimate of a one-dimensional (1D) approach of the tunneling factor in the reaction instead of calculating the analytical potential energy surface, which is very important for determination of the reaction rate constants. In addition, Rayez et al. did not report the rate constants at the other temperatures besides 298 K. Our results within 200−700 K may present a useful comparison for further experiments.

From Figure 3a, we can also see that the variational effect is large and the small-curvature tunneling effect is small on the rate constants for the $CHCl_3$ reaction. From Figure 3b−d, we can easily find that the curves of TST, ICVT, and ICVT/SCT are nearly the same, which indicates that the variational effect

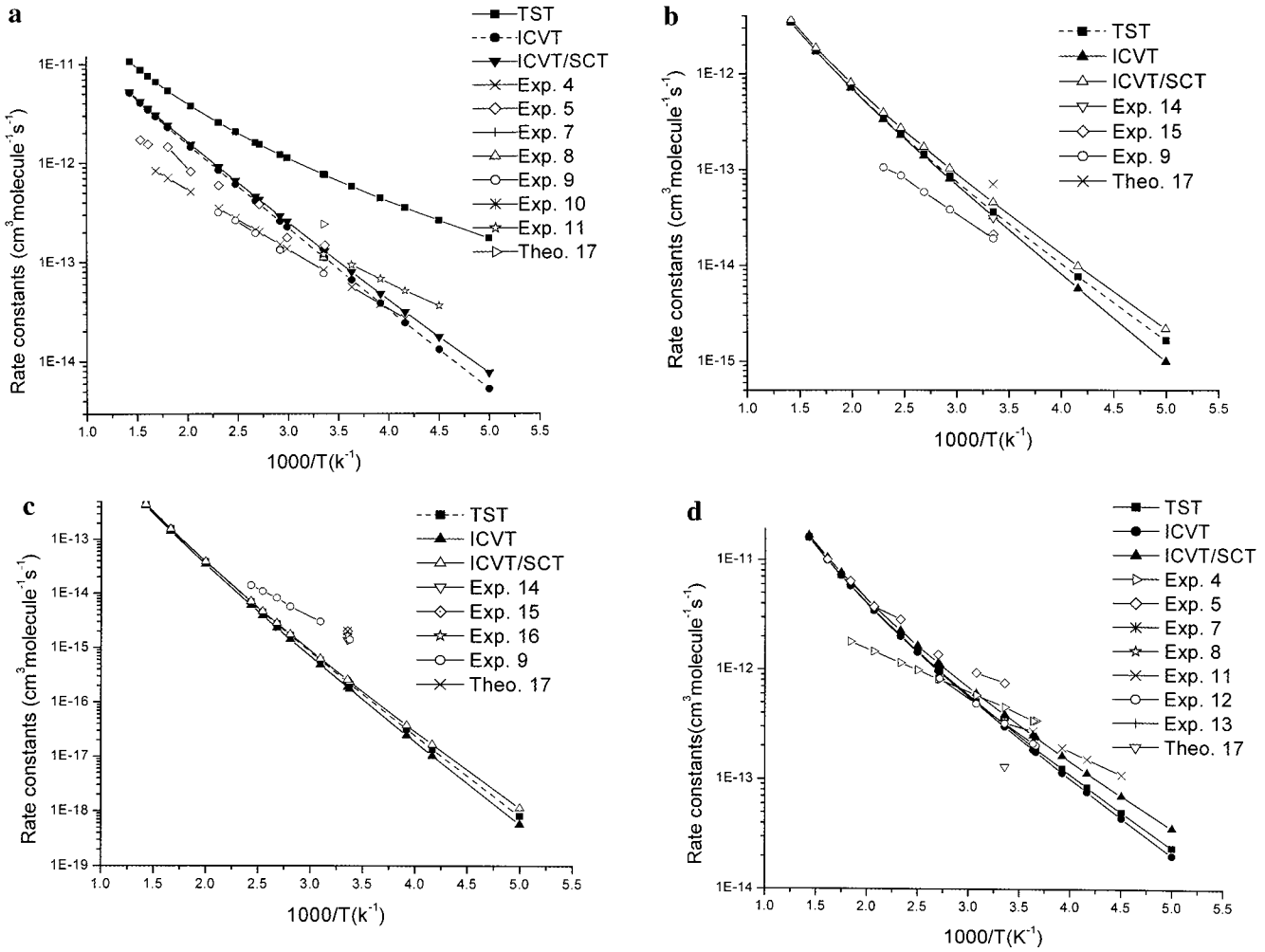

Figure 3. Computed TST, ICVT, and ICVT/SCT rate constants as a function of $10^3/T$ and available experimental values for the (a) $CHCl_3 + Cl \rightarrow CCl_3 + HCl$, (b) $CHCl_2F + Cl \rightarrow CCl_2F + HCl$, (c) $CHClF_2 + Cl \rightarrow CClF_2 + HCl$, and (d) $CH_2Cl_2 + Cl \rightarrow CHCl_2 + HCl$ reactions.

TABLE 5: ICVT and ICVT/SCT Forward Reaction Rate Constants (cm^3 $molecule^{-1}$ s^{-1}) for the Selected Hydrogen Abstraction Reactions

	$CHCl_3 + Cl \rightarrow CCl_3 + HCl$		$CHCl_2F + Cl \rightarrow CCl_2F + HCl$		$CHClF_2 + Cl \rightarrow CClF_2 + HCl$		$CH_2Cl_2 + Cl \rightarrow CHCl_2 + HCl$	
T (K)	ICVT	ICVT/SCT	ICVT	ICVT/SCT	ICVT	ICVT/SCT	ICVT	ICVT/SCT
200.0	5.28×10^{-15}	7.66×10^{-15}	9.99×10^{-16}	2.19×10^{-15}	5.72×10^{-19}	1.14×10^{-18}	2.03×10^{-14}	3.60×10^{-14}
250.0	3.30×10^{-14}	4.15×10^{-14}	8.16×10^{-15}	1.33×10^{-14}	1.85×10^{-17}	2.88×10^{-17}	1.01×10^{-13}	1.46×10^{-13}
298.0	1.12×10^{-13}	1.32×10^{-13}	3.21×10^{-14}	4.51×10^{-14}	1.86×10^{-16}	2.54×10^{-16}	3.00×10^{-13}	3.87×10^{-13}
300.0	1.17×10^{-13}	1.37×10^{-13}	3.37×10^{-14}	4.71×10^{-14}	2.02×10^{-16}	2.75×10^{-16}	3.12×10^{-13}	4.01×10^{-13}
350.0	2.93×10^{-13}	3.29×10^{-13}	9.52×10^{-14}	1.22×10^{-13}	1.18×10^{-15}	1.48×10^{-15}	7.28×10^{-13}	8.75×10^{-13}
400.0	5.84×10^{-13}	6.38×10^{-13}	2.13×10^{-13}	2.57×10^{-13}	4.62×10^{-15}	5.50×10^{-15}	1.43×10^{-12}	1.64×10^{-12}
450.0	1.00×10^{-12}	1.07×10^{-12}	4.11×10^{-13}	4.77×10^{-13}	1.39×10^{-14}	1.59×10^{-14}	2.49×10^{-12}	2.78×10^{-12}
500.0	1.55×10^{-12}	1.64×10^{-12}	7.11×10^{-13}	8.02×10^{-13}	3.44×10^{-14}	3.85×10^{-14}	4.00×10^{-12}	4.37×10^{-12}
600.0	3.04×10^{-12}	3.16×10^{-12}	1.72×10^{-12}	1.86×10^{-12}	1.43×10^{-13}	1.55×10^{-13}	8.63×10^{-12}	9.19×10^{-12}
700.0	5.12×10^{-12}	5.27×10^{-12}	3.42×10^{-12}	3.63×10^{-12}	4.22×10^{-13}	4.47×10^{-13}	1.59×10^{-11}	1.67×10^{-11}

and small-curvature tunneling effect are small on the rate constants for the $CHCl_2F$, $CHClF_2$, and CH_2Cl_2 reactions. The variational effect discrepancies may originate from the flat V_{MEP} with a lower classical barrier height for reaction $CHCl_3 + Cl$ compared to the other three reactions, as is discussed in section 3.B. The small-curvature tunneling effect on the rate constants can also be reflected in Table 5. Particularly, for the reactions $CHCl_3 + Cl$ and $CH_2Cl_2 + Cl$, the ratio k(ICVT/SCT)/k(ICVT) falls within the range 1.03−1.45 and 1.05−1.77, respectively.

In the above discussions, the small curvature tunneling (SCT) correction is used. Yet, when the reaction path is acutely curved, as in the H-abstraction between two heavy fragments, the contribution from the large curvature tunneling (LCT) correction should be considered especially at low temperatures.[27] For a typical reaction $A + BC \rightarrow AB + C$, the skewed angle θ of the reaction path curvature is defined by the expression $\cos\theta = \sqrt{m_A m_C/(m_A+m_B)(m_B+m_C)}$ (m is the effective mass.). For the H-abstraction reactions $CHCl_3 + Cl$, $CHCl_2F + Cl$, $CHClF_2 + Cl$, and $CH_2Cl_2 + Cl$, the θ value is small as 10.9°, 11.1°, 11.4°, and 11.4°, respectively. This indicates that the large curvature tunneling may have some influence on the calculation of the rate constants for the four title reactions. Unfortunately, the LCT correction can only be made where an analytic representation of the potential energy surface (PES) for a reaction is available.[36] Different from the SCT effect, the LCT effect cannot be directly calculated by means of the ab initio PES. Since the skewed angle θ is almost the same, the LCT

effect is expected to be similar for the four H-abstraction reactions; i.e., inclusion of LCT may not change the qualitative results for the four reactions. Moreover, while our calculated rate constants with SCT correction are in good agreement with available experimental values, we expect that the LCT effect correction may not change quantitatively the results too much.

Conclusions

In this paper, the hydrogen abstraction reactions from $CHCl_{3-n}F_n$ ($n = 0-2$) and CH_2Cl_2 by chlorine atoms are investigated theoretically. Dynamical calculations are based on a full improved canonical variational transition state theory plus multidimensional semiclassical tunneling correction with the potential energies information calculated directly from a combination of QCISD(T) and BH&H-LYP DFT methods. It is found that the classical barrier height for the H-abstraction reactions is in the order $CHCl_3 < CH_2Cl_2 < CHCl_2F < CHClF_2$, whereas the exothermicities of the reactions decrease in the opposite order. By analyzing the reaction path of the title reactions, it is shown that the vibrational adiabatic potential energy curves for the title reactions have two barriers, a situation similar to the analogous reactions CH_3X (X = F, Cl, and Br) + Cl.

The calculated rate constants of these reactions are in good agreement with the experimental values over the measured temperature range, although the theoretical temperature dependence of rate constants is slightly steeper than the experimental ones. It is found that the variational effect is significant for the $CHCl_3$ + Cl reaction and small-curvature tunneling effects are small on the rate constants for all the title reactions. Our theoretical results may be useful for further revealing the dynamical properties of this kind of hydrogen abstraction reaction.

Acknowledgment. We thank Professor Donald G. Truhlar for providing the POLYRATE 8.4.1 program. This work is supported by the National Science Foundation of China (29892168, 200073014), Doctor Foundation by the Ministry of Education, Foundation for University Key Teacher by the Ministry of Education, and Key subject of Science and Technology by the Ministry of Education of China.

References and Notes

(1) (a) Tuck, R.; Plumb, A.; Condon, E. *Geophys. Res. Lett*. **1990**, *17*, 313. (b) Rosswall, T. *Environ. Sci. Technol*. **1991**, *25*, 567.

(2) (a) Atkinson, R. *Chem. Rev*. **1986**, *86*, 69. (b) Atkinson, R. *J. Phys. Chem. Ref. Data*. **1994**, Monograph 2.

(3) Senkan, S. M. *Environ. Sci. Technol*. **1988**, *22*, 368.

(4) Knox, J. H. *Trans. Faraday. Soc*. **1962**, *58*, 275.

(5) Clyne, M. A. A.; Walker, R. F. *J. Chem. Soc. Faraday. Trans. 1* **1973**, *69*, 1547.

(6) Atkinson, R.; Baulch, D. L.; Cox, R. A.; Hampson, R. F.; Keer, J. A.; Troe, J. *J. Phys. Chem. Ref. Data.* **1992**, *21* (6), 1125.

(7) Beichert, P.; Wingen, J. L.; Vogt, R.; Ezell, M. J.; Ragains, M.; Neavyn, R.; Finlayson-Pitts, B. J. *J. Phys. Chem.* **1995**, *99*, 13156.

(8) Catoire, V.; Lesclaux, R.; Schneider, W. F.; Wallington, T. J. *J. Phys. Chem.* **1996**, *100*, 14356.

(9) Talhaoui, A.; Louis, F.; Meriaux, B.; Devolder, P.; Sawerysyn, J. P. *J. Phys. Chem.* **1996**, *100*, 2107.

(10) Brahan, K. M.; Hewitt, A. D.; Boone, G. D.; Hewitt, S. A. *Int. J. Chem. Kinet*. **1996**, *28*, 397.

(11) Orlando, J. J. *Int. J. Chem. Kinet*. **1999**, *31*, 515.

(12) Tschuikow-Roux, E.; Faraji, F.; Paddison, S.; Niedzielski, J.; Miyokawa, K. *J. Phys. Chem*. **1988**, *92*, 1488.

(13) Niki, H.; Maker, P. D.; Savage, C. M.; Breitenbach, L. P. *Int. J. Chem. Kinet*. **1980**, *12*, 1001.

(14) Jourdain, G. L.; Poulet, G.; Barassin, J.; Lebras, G.; Combourieu, J. *J. Pollut. Atmos*. **1977**, *75*, 256.

(15) Tauzon, E. C.; Atkinson, R.; Corchnoy, S. B. *Int. J. Chem. Kinet*. **1992**, *24*, 639.

(16) Sawerysyn, J. P.; Talhaoui, A.; Meriaux, B.; Devolder, P. *Chem. Phys. Lett*. **1992**, *198*, 197

(17) Rayez, M. T.; Rayez, J. C.; Sawerysyn, J. P. *J. Phys. Chem*. **1994**, *98*, 11342.

(18) Duncan, W. T.; Truong, T. N. *J. Chem. Phys*. **1995**, *103*, 9642.

(19) Truong, T. N.; Duncan, W. T.; Bell, R. L. In *Chemical Applications of Density-Functional Theory*; Americal Chemical Society: Washington, DC, 1996; p 85.

(20) Truong, T. N. *J. Chem. Phys*. **1994**, *100*, 8014.

(21) Maity, D. K.; Duncan, W. T.; Truong, T. N. *J. Phys. Chem. A* **1999**, *103*, 2152.

(22) Becke, A. D. *J. Chem. Phys*. **1993**, *98*, 1372.

(23) Lee, C.; Yang, W.; Parr, R. G. *Phys. Rev. B* **1988**, *37*, 785.

(24) Frisch, M. J.; Trucks, G. W.; Schlegel, H. B.; Scuseria, G. E.; Robb, M. A.; Cheeseman, J. R.; Zakrzewski, V. G.; Montgomery, J. A., Jr.; Stratmann, R. E.; Burant, J. C.; Dapprich, S.; Millam, J. M.; Daniels, A. D.; Kudin, K. N.; Strain, M. C.; Farkas, O.; Tomasi, J.; Barone, V.; Cossi, M.; Cammi, R.; Mennucci, B.; Pomelli, C.; Adamo, C.; Clifford, S.; Ochterski, J.; Petersson, G. A.; Ayala, P. Y.; Cui, Q.; Morokuma, K.; Malick, D. K.; Rabuck, A. D.; Raghavachari, K.; Foresman, J. B.; Cioslowski, J.; Ortiz, J. V.; Boboul, A. G.; Stefnov, B. B.; Liu, G.; Liashenko, A.; Piskorz, P.; Komaromi, I.; Gomperts, R.; Martin, R. L.; Fox, D. J.; Keith, T.; Al-Laham, M. A.; Peng, C. Y.; Nanayakkara, A.; Gonzalez, C.; Challacombe, M.; Gill, P. M. W.; Johson, B.; Chen, W.; Wong, M. W.; Andres, J. L.; Gonzalez, C.; Head-Gordon, M.; Replogle, E. S.; Pople, J. A. *Gaussian 98w*, Revision A.7; Gaussian, Inc.: Pittsburgh, PA, 1998.

(25) Pople, J. A.; Head-Gordon, M.; Raghavachari, K. *J. Chem. Phys*. **1987**, *87*, 5968.

(26) Chang, Y.-Y.; Corchado, J. C.; Fast, P. L.; Villa, J.; Hu, W.-P.; Liu, Y.-P.; Lynch, G. C.; Jackels, C. F.; Nguyen, K. A.; Gu, M. Z.; Rossi, I.; Coitino, E. L.; Clayton, S.; Melissas, V. S.; Lynch, B. J.; Steckler, R.; Garrett, B. C.; Isaacson, A. D.; Truhlar, D. G. *POLYRATE*, version 8.4.1; University of Minnesota: Minneapolis, 2000.

(27) Truhlar, D. G.; Isaacson, A. D.; Garrett, B. C. Generalized Transition State Theory. In *The Theory of Chemical Reaction Dynamics*; Baer, M., Ed.; CRC Press: Boca Raton, FL, 1985; Vol. 4, p 65.

(28) Steckler, R.; Hu, W.-P.; Liu,Y.-P.; Lynch, G. C.; Garrett, B. C.; Isaacson, A. D.; Melissas, V. S.; Lu, D.-P.; Troung, T. N.; Rai, S. N.; Hancock, G. C.; Lauderdale, J. G.; Joseph, T.; Truhlar, D. G. *Comput. Phys. Commun.* **1995**, *88*, 341.

(29) Huber, K. P.; Herzberg, G. *Molecular Spectra and Molecular Structure. IV. Constants of Diatomic Molecules*; Van Nostrand Reinhold Co.: New York, 1979.

(30) Milligan, D. E.; Jacox, M. E.; McAuley, J. H.; Smith, C. E. *J. Mol. Spectrosc*. **1973**, *45*, 377.

(31) Chase, M. W., Jr.; Davies, C. A.; Downey, J. R., Jr.; Frurip, D. J.; McDonald, R. A.; Syverud, A. N. In *JANAF Thermochemical Tables*, 3rd ed.; Journal of Physical and Chemical Reference Data; American Chemical Society and the American Institute of Physics for the National Bureau of Standards, 1985; Vol. 14, Suppl. 1.

(32) In *NIST Chemistry WebBook*, NIST Standard Reference database Number 69, February 2000 Release. Vibrational frequency data compiled by M. E. Jacox.

(33) DeMore, W. B.; Sander, S. P.; Golden, D. M.; Hampson, R. F.; Kurylo, J.; Howard, C. J.; Ravishankara, A. R.; Kolb, C. E.; Molina, M. J. JPL Publication 92-20; Jet Propulsion Laboratory: Pasadena. CA, 1992.

(34) Rosenman, E.; McKee, M. L. *J. Am. Chem. Soc*. **1997**, *119*, 9033.

(35) Xiao, J. F.; Li, Z. S.; Ding, Y. H.; Huang, X. R.; Sun, C. C. *Phys. Chem. Chem. Phys*., in press.

(36) Hand, M. R.; Rodriquez, C. F.; Williams, I. H.; Balint-Kurti, G. G. *J. Phys. Chem. A* **1998**, *102*, 5958.